JOURNAL OF Applied Polymer SCIENCE

Thermotropic Systems with Fixed Domains Exhibiting Enhanced Overheating Protection Performance

Andreas Weber,[1] Katharina Resch[2]

[1]Polymer Competence Center Leoben GmbH, Roseggerstrasse 12, 8700 Leoben, Austria

[2]Materials Science and Testing of Polymers, Department Polymer Engineering and Science, University of Leoben, Otto Glöckel-Strasse 2, 8700 Leoben, Austria

Correspondence to: K. Resch (E-mail: katharina.resch@unileoben.ac.at)

ABSTRACT: Within this study, a time saving photo-initiated miniemulsion polymerization process (duration of polymerization was 15 min) was established in order to encapsulate a paraffin wax with an acrylate polymer shell. The obtained freeze-dried latex was an off-white powder exhibiting spherical particles with mean diameters around 400 nm and a concentration of paraffin wax around 56%. Mixing the reaction product with a UV-curable resin matrix resulted in thermotropic overheating protection glazings with high light-shielding efficiency. © 2014 Wiley Periodicals, Inc. J. Appl. Polym. Sci. **2014**, *131*, 40417.

KEYWORDS: emulsion polymerization; differential scanning calorimetry; nanoparticles; nanowires and nanocrystals; optical and photovoltaic applications; photopolymerization

Received 12 November 2013; accepted 9 January 2014

DOI: 10.1002/app.40417

INTRODUCTION

Thermotropic glazings change their optical properties from transparent to opaque upon exceeding a predefined threshold temperature, reversibly.[1,2] Thus, they can provide efficient overheating protection for buildings as well as for solar thermal collectors.[1,3–9] Upon utilization in a building's façade, a reduction in primary energy demand is achievable by reduction of energy consumption for heating, cooling, and artificial daylighting.[3,4] In solar thermal collectors, they can limit stagnation temperatures to values below 130°C, which otherwise would exceed 180°C and thus prevent deterioration, aging, and potential failure of heat carrier fluid and other collector components.[9–11] Especially, for polymeric solar thermal systems stagnation control is a prerequisite in order not to exceed the long-term service temperatures of utilized—preferably cost-efficient—polymeric materials.[9,10,12,13]

Besides other thermotropic glazing systems, thermotropic systems with fixed domains (TSFD) are promising due to specific advantages like ease of adjustment of switching threshold, high long-term stability, low hysteresis, high reversibility, and steep switching process.[8] The TSFD itself consist of a thermotropic additive finely dispersed in a matrix material.[1,6] Below the threshold temperature, the refractive indices of both components are almost equal, enabling the incident radiation to pass the layer almost un-scattered.[1] Upon exceeding the threshold temperature (i.e., melting of the additive), the refractive index of the thermotropic additive exhibits a steep change.[1] Thus a significant refractive index difference between matrix and additive is obtained, finally resulting in intense scattering of incident radiation.[1] Besides refractive index difference, layer morphology governs overheating protection of TSFD to a high extent.[14,15] Most efficient light-shielding is achieved for spherical scattering domains with diameters between 200 and 400 nm.[14] Notwithstanding, the achieved light-shielding efficiency of TSFD established so far is limited, and especially inappropriate for efficient overheating protection of an all-polymeric flat plate collector.[8,9,13,16–24] Primarily, this was attributed to inappropriate scattering domain shape and/or size.[13,17,19–23,25,26] Scattering domains were either spherical or nonspherical but too big in general anyway. In 2008, Resch[27] suggested adjustment of scattering domain shape and size prior to TSFD formulation in order to enhance overheating protection performance of TSFD. To the best of our knowledge, Muehling et al.[24] were the first and only ones so far conducting a study devoted to the establishment of properly sized scattering domains for TSFD formulation. However, the established threshold temperature (25°C[24]) is rather low and thus not appropriate for overheating protection of a solar thermal collector. Overheating protection of a solar thermal collector either requires threshold temperatures in the range between 55 and 60°C or 75 and 80°C, respectively.[9] Thus, an objective of this study was to establish a novel process for adjustment of scattering domain size of thermotropic additives with rather high melting point (i.e., 55°C). Furthermore,

formulation of TSFD with these optimally sized scattering domains was an issue.

ENCAPSULATION OF THERMOTROPIC ADDITIVE

Background

As suggested earlier,[21,24] encapsulation of thermotropic additive was considered a promising approach for adjustment of scattering domain size in order to formulate TSFD with efficient overheating protection performance. Therefore, the considerations that led to the actual setup of the subsequently employed encapsulations process are outlined in the following paragraphs.

For encapsulation of phase change materials in general and alkanes and paraffin waxes—which may also serve as thermotropic additives—more specifically, polymerization processes employing vinyl monomers are addressed rather frequently in Refs. 28–50. However, besides other techniques, the most versatile process to establish encapsulated thermotropic additive with controlled size is probably miniemulsion polymerization.[36,51–64] In miniemulsion polymerization the polyreactions take place in some kind of "nanoreactors" formed by the disperse phase, which are separated from each other by the continuous phase.[55,57,65] Extensive reviews on the details of miniemulsion polymerization—also for encapsulation purposes—are presented elsewhere.[55,57,58,61,65,66] One noteworthy aspect of miniemulsion polymerization is that the "nanoreactor"-droplets have to be stabilized against growth due to Ostwald-ripening by addition of an ultrahydrophobe.[55,57,65] For example, the alkane hexadecane was recognized as a very efficient ultrahydrophobe.[55,65] This is very interesting because with regard to adjustment of the switching threshold of a TSFD, alkanes, and paraffin waxes are probably the most versatile thermotropic additives because of rather easy availability of materials displaying a melting transition in the desired temperature ranges (either 55–60°C or 75–80°C[9]). Hence, upon miniemulsion polymerization mediated encapsulation of an alkane or a paraffin wax these substances act as an ultrahydrophobe simultaneously.

However, encapsulation of paraffin waxes exhibiting melting in the previously specified temperature ranges might encounter challenges that are related to standard thermal initiation of miniemulsion polymerization: To form an emulsion, usually the water- and the oil-phase are assembled separately prior to emulsification.[35,36,63] Thereby, the oil-phase contains the monomers (e.g., acrylates) and the paraffin wax (simultaneously acting as ultrahydrophobe in miniemulsion polymerization). Both phases have to be heated above the melting temperature of the paraffin wax in order to subsequently establish an oil-in-water (O/W) emulsion. High energy emulsification techniques (e.g., ultrasound) are required in order to establish a miniemulsion with narrow size distribution and small mean diameter.[24,57,65,67–69] However, the high temperatures employed prior, during and after emulsification and heat dissipation due to emulsification might be a challenge for thermal initiators, especially for oil-soluble ones. Oil-soluble initiators have to be mixed with the oil-phase prior to emulsification.[36] This may cause uncontrollable polymerization start due to decomposition of the thermal initiator when exposed to high temperatures during establishment of the miniemulsion. Utilization of water soluble initiators, which can be added after emulsification and thus may overcome the previously mentioned shortcomings of oil soluble initiators, is not an option when utilizing rather water soluble monomers like methyl methacrylate (MMA). Otherwise nucleation in the aquatic phase and subsequent growth of pure polymer particles (e.g., PMMA) might occur,[63] which is undesirable when performing an encapsulation process.

Thus, decoupling the polymerization initiation from the reactants' temperatures was considered to be an imperative in order to facilitate utilization of oil soluble initiator while maintaining spatial and temporal control of initiation reaction. That may be achieved via photo-initiation of the polymerization process.[54,70] Furthermore, photo-initiation might provide additional advantages as compared to thermal initiation, like high reaction rates and feasibility of photo-initiated processes for continuous reactors.[70] Thus, the miniemulsion polymerization process for encapsulation is considered to be significantly accelerated by substitution of thermal initiation (e.g., reactions last around 3 h in Ref. 24) by photo-initiation. However, photo-initiation for starting polymerization within an encapsulation process of phase change materials was rarely addressed in the past.[37,46]

Anyway, not virtually any monomer is suitable for encapsulation of paraffin wax intended for use as scattering domain in a TSFD. A proper match of refractive indices (n) of the core and the polymeric shell is required for this purpose. For paraffin waxes ($n \sim 1.5$), polymers with a proper match of refractive index are derived from acrylate monomers, e.g., Poly(methyl methacrylate) (PMMA; $n = 1.49$) or Poly (isobornyl methacrylate) (PiBoMA; $n = 1.50$).[20,71–73] Furthermore, polymers based on acrylate esters are recognized rather stable upon exposition to UV-light.[74]

Experimental

Materials. Monomers methyl methacrylate (MMA; 99%), ethylene glycol dimethacrylate (EGDMA; 98%), isobornyl methacrylate (iBoMA; technical grade) and surfactant sodium lauryl sulfate (SDS; ≥98.5%) were purchased from Sigma Aldrich Handels GmbH (Wien, AT). Thermotropic additive paraffin wax (Sasolwax 5005) and photo-initiator (Lucirin TPO-L) were supplied by Sasol Wax GmbH (Hamburg, DE) and BASF SE (Ludwigshafen, DE), respectively. All materials were used as received.

Miniemulsion Polymerization. Monomer mixture either consisted of 4.5 g MMA and 0.5 g EGDMA or 2.5 g MMA, 2.0 g iBoMA and 0.5 g EGDMA. The oil phase was assembled by mixing and stirring the monomer mixture (5 g), paraffin wax (5 g), and photo-initiator Lucirin TPO-L (0.15 g) in a beaker immersed in an oil bath (temperature: 70°C) until it was clear. The water phase was established by mixing SDS with 50 g deionized water in a beaker also immersed in the oil bath. The required amount of SDS was evaluated in preliminary tests. A concept estimating the area a single surfactant molecule is stabilizing in an emulsion (A_{surf}; see Refs. 52,53,60,75,76) was adopted in order to estimate a reasonable starting concentration of surfactant for these tests. Preliminary tests revealed an amount of 8.3 mg SDS to be effectual. To form the emulsion, the oil phase was transferred to the beaker (made from clear

Schott DURAN glass) with the water phase and subsequently emulsified by ultrasound from a Sonopuls HD 3200 equipped with a booster horn SH 213 G and a sonotrode KE76 (Bandelin electronic GmbH & Co. KG, Berlin, DE), maintaining an amplitude set-point of 70% for 5 min. Subsequently, the established emulsion was irradiated through the beaker wall for 900 s at 100% intensity with radiation from a light-guide attached to OmniCure S 1000 (Lumen Dynamics Group, Mississauga, ON). During irradiation vigorous stirring with a magnetic stirrer bar and continuous nitrogen flow was maintained. The obtained dispersion was freeze-dried.

Freeze-Drying. Proof of concept for freeze-drying was established via a laboratory apparatus consisting of a vacuum pump P8Z (Ilmvac GmbH, Illmenau, DE) equipped with a vacuum control unit, a cooling trap cooled with liquid nitrogen and a salt/water/ice-bath for immersion of the round-bottomed flask with the frozen latex. Larger amount of dried latex was obtained by utilizing a commercial freeze-dryer Alpha 2-4 (Martin Christ Gefriertrocknungsanlagen GmbH, Osterode am Harz, DE) equipped with a rotary vane pump RV 5 (Edwards, Crawley, West Sussex, GB).

Capsule Characterization. To prove evidence for successfully conducted polymerization reaction, infrared (IR) spectra of freeze-dried latex were recorded in mode of attenuated total reflection (ATR) employing a Spectrum GX FTIR spectrometer (Perkin Elmer, Waltham, MA) equipped with an ATR device GladiATR Vision (PIKE Technologies, Madison, WI).

Thermal transitions and melting enthalpies of pristine paraffin wax and of encapsulated wax were determined by differential scanning calorimetry (DSC). Thermograms were recorded under nitrogen flow (40 mL min^{-1}) on a DSC 4000 (Perkin Elmer, Waltham, MA) applying a heating/cooling rate of 10 K min^{-1} in the range between −20 and 100°C. Sample mass was 10 ± 1 mg. Threefold determination was carried out for each sample. Melting temperature (peak temperature) and enthalpy of melting transition were evaluated from the second heating run. Mass content of paraffin wax (w_{Core}) in the capsules was calculated by building the ratio of the specific melting enthalpy of the capsules ($h_{Capsules}$ in J g^{-1}) and the specific melting enthalpy of the pristine paraffin wax ($h_{Core\ material}$ in J g^{-1}) [eq. (1)].

$$w_{Core} = \frac{h_{Capsules}}{h_{Core\,material}} \quad (1)$$

After transferring the particles to a sample mount and subsequent sputtering with gold, capsule morphology was characterized employing scanning electron microscope (SEM) DSM 962 (Carl Zeiss SMT AG, Oberkochen, DE). Capsule size was evaluated with measurement tools of software analySIS (Soft Imaging System GmbH, Münster, DE). From the capsule diameters ($d_{Capsule}$), the core diameters (d_{Core}) were calculated according to eq. (2). Density of the core material paraffin wax (ρ_{Core}) and the polymeric shell (ρ_{Shell}) were assumed to be 0.91 (value for a paraffin with melting point around 55°C[77]) and 1.19 g cm^{-3} (value for PMMA[78–80]), respectively.

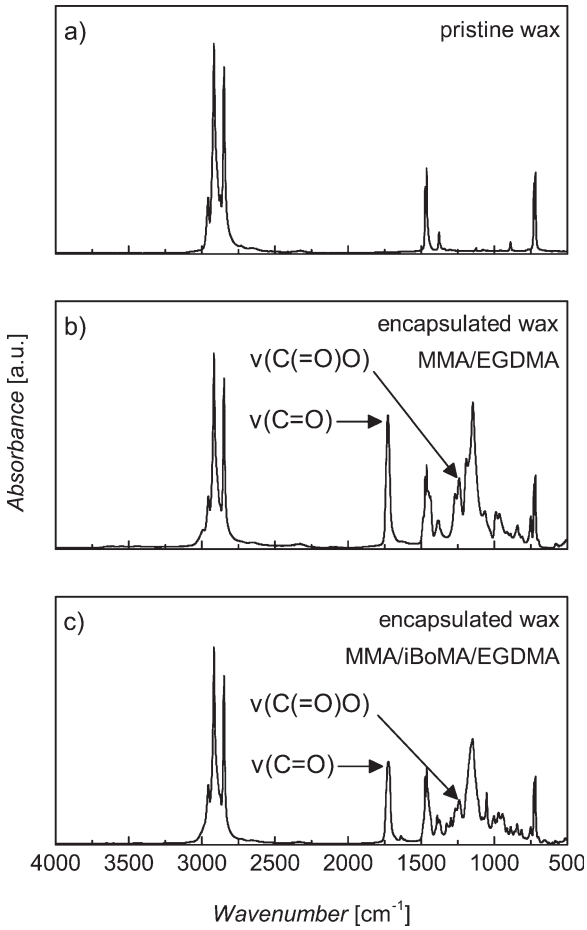

Figure 1. ATR-spectra of (a) pristine wax, encapsulated wax with a polymeric shell obtained from (b) MMA and EGDMA, or (c) MMA, iBoMA, and EGDMA.

$$d_{Core} = d_{Capsule} * \left(1 + \frac{\rho_{Core}}{\rho_{Shell}} * \frac{1 - w_{Core}}{w_{Core}}\right)^{-1/3} \quad (2)$$

The core diameter was calculated because it was of major interest with regard to the light-shielding efficiency of TSFD formulated with the obtained capsules. In contrast, the outer diameter of the protective shell of the additive core was of minor interest. Size distribution histograms were established with graphical statistics tool of software Origin 9.0 (OriginLab Corporation, Northampton, MA).

RESULTS

In Figure 1 the ATR spectra of pristine paraffin wax [Figure 1(a)], and of encapsulated paraffin wax with a polymeric shell obtained from either, MMA and EGDMA [Figure 1(b)], or MMA, iBoMA, and EGDMA [Figure 1(c)] are displayed. Band assignment is based on information provided by Refs. 81–84. The bands identified for pristine wax were: IR (ATR): ν = 2957 (m, $\nu_{as}(CH_3)$), 2917 (vs, $\nu_{as}(CH_2)$), 2874 (w, $\nu_s(CH_3)$), 2849 (vs, $\nu_s(CH_2)$), 1473 (m, $\delta_s(CH_2)$), 1463 (s, $\delta_s(CH_2)$, $\delta_{as}(CH_3)$), 1378 (w, $\delta_s(CH_3)$), 730 (m, $\rho(CH_2)$), 719 cm^{-1} (s, $\rho(CH_2)$). These bands were also identified for the paraffin wax encapsulated with a shell of either MMA and EGDMA or MMA, iBoMA and

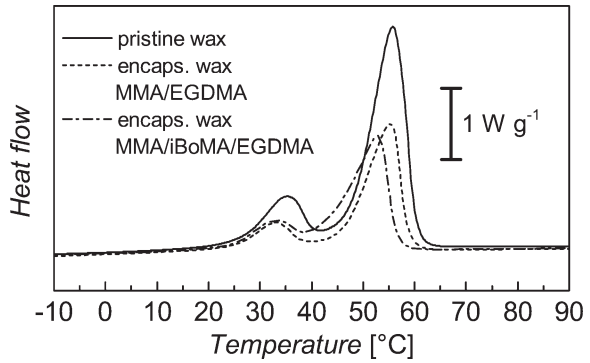

Figure 2. DSC-thermograms (second heating run) of pristine wax (solid line), encapsulated wax with a polymeric shell obtained from MMA and EGDMA (dotted line), or MMA, iBoMA, and EGDMA (dash-dotted line).

Table I. Specific Melting Enthalpies for Paraffin Wax Encapsulated with a Polymeric Shell Obtained from MMA and EGDMA or from MMA, iBoMA, and EGDMA and Resultant Paraffin Wax Content of the Capsules (w_{Core}) Calculated Based on the Specific Melting Enthalpy of the Pristine Wax $h_{Core\ Material}$ = 204 J g^{-1}

Monomer mixture	$h_{Capsules}$ (J g^{-1})	w_{Core} (%)
MMA/EGDMA	112	55
MMA/iBoMA/EGDMA	117	57

EGDMA. Further bands identified for both encapsulated products were: IR (ATR): ν = 1728 (s, ν(C═O)), 1240 (m, ν(C(═O)O)), 1147 (s, ρ'(CH_3)), 988 (w, ν(O─C)), 750 cm^{-1} (w, δ(C═O)). Especially, the bands ascribed to the carbonyl-moieties (e.g., at 1240 cm^{-1}) gave evidence for successfully conducted polymerization. For the product encapsulated with MMA, iBoMA, and EGDMA two more bands were evident, which were not detectable or at least much weaker for the product encapsulated with MMA and EGDMA: IR(ATR): ν = 1327 (w, probably a C─H deformation vibration of a ternary C─H group), 1052 cm^{-1} (probably a C─C skeletal vibration of >$C(CH_3)_2$), both indications for the isobornyl-group being present.

In Figure 2 the second DSC heating runs recorded for pristine paraffin wax (solid line), and encapsulated paraffin wax with a polymeric shell obtained from either, MMA and EGDMA (dotted line), or MMA, iBoMA, and EGDMA (dash-dotted line) are depicted. Melting peak temperatures of paraffin wax were 56°C for the pristine wax, 55°C for the wax encapsulated with a polymeric shell resulting from MMA and EGDMA and 53°C for the wax encapsulated with a polymeric shell resulting from MMA, iBoMA, and EGDMA, respectively. The specific melting enthalpies obtained from these thermograms are listed in Table I. Whereas the pristine paraffin wax had a specific melting enthalpy of 204 J g^{-1} ($h_{Core\ Material}$), the wax encapsulated with a shell of MMA and EGDMA displayed a specific melting enthalpy of 112 J g^{-1}. Thus, according to eq. (1), the related freeze dried product contained 55% paraffin wax. For the paraffin wax encapsulated with a shell of MMA, iBoMA, and EGDMA the specific melting enthalpy was 117 J g^{-1}, yielding a wax content of 57%.

Figures 3 and 4 displays SEM micrographs of the paraffin wax encapsulated with a polymeric shell obtained from either MMA and EGDMA (Figure 3) or MMA, iBoMA and EGDMA (Figure 4) in magnifications of 10,000 [Figures 3 and 4(a)] and 30,000 [Figures 3 and 4(b)]. Micrographs display aggregated spherical particles. A survey of individual particles from numerous micrographs enabled establishment of particle size distributions. Furthermore, for each individual particle the calculation of a hypothetical core diameter [according to eq. (2); assumption: uniform wax content for all particles] was carried out. The resulting size distribution histograms are depicted in Figures 5 and 6. For illustration purposes, a logarithmic normal-

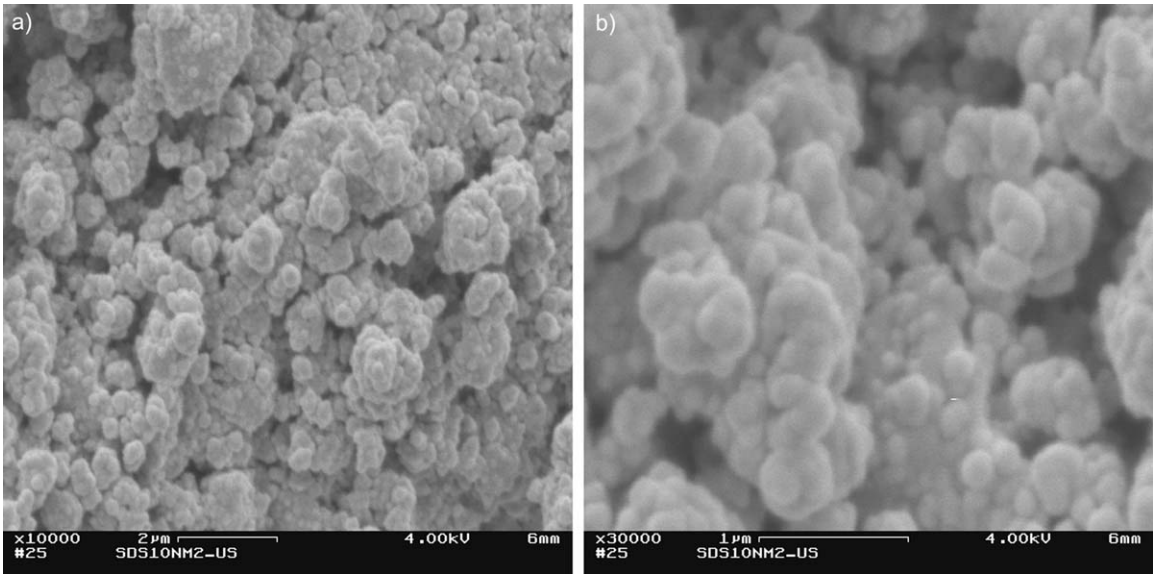

Figure 3. SEM micrographs of paraffin wax encapsulated with a polymeric shell obtained from MMA and EGDMA. Magnifications displayed are (a) 10,000× and (b) 30,000×.

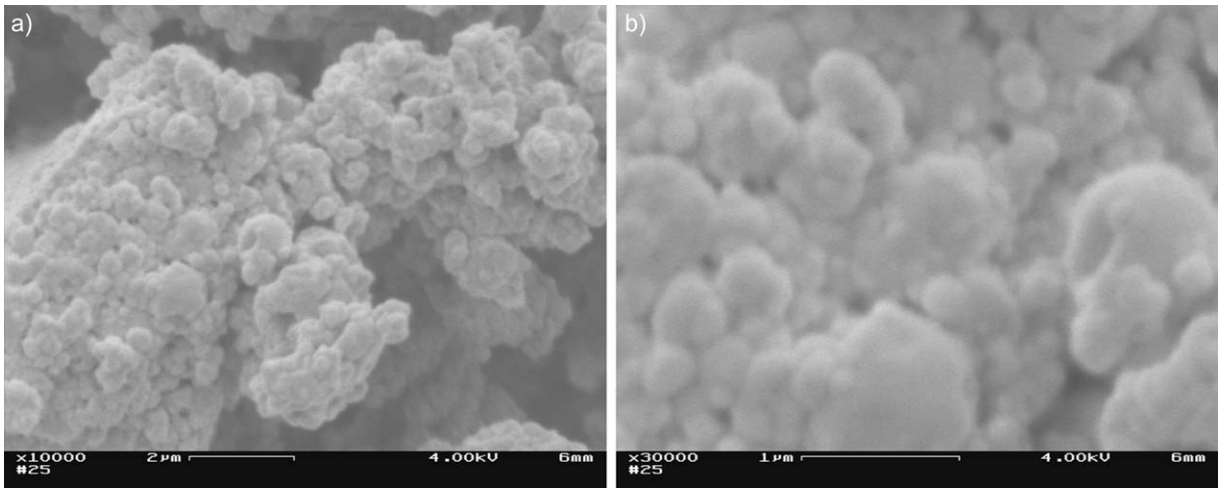

Figure 4. SEM micrographs of paraffin wax encapsulated with a polymeric shell obtained from MMA, iBoMA, and EGDMA. Magnifications displayed are (a) 10,000× and (b) 30,000×.

distribution curve was overlaid on the histograms. The mean and median of the actually detected particle diameters for the wax encapsulated with a shell resulting from MMA and EGDMA were 354 and 280 nm, respectively [histogram see Figure 5(a)]. The size distribution of the core diameters exhibited mean and median of 301 and 238 nm, respectively [histogram see Figure 5(b)]. The vast majority of the particle cores had diameters between 50 and 1000 nm. The mean and median of the actually detected particle diameters for wax encapsulated with a shell resulting from MMA, iBoMA, and EGDMA were 487 and 439 nm, respectively [histogram see Figure 6(a)]. The size distribution of the core diameters exhibited mean and median of 419 and 377 nm, respectively [histogram see Figure 6(b)]. The vast majority of these particle cores had diameters between 100 and 1000 nm. Table II summarizes the key findings of the particle characterization.

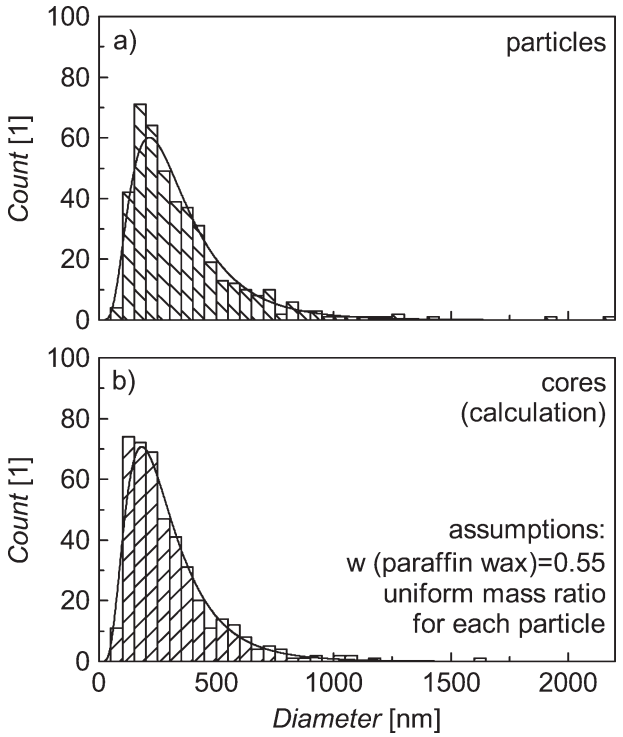

Figure 5. Histograms and overlaid logarithmic normal-distribution of (a) diameters of particles with a wax core and a shell made of MMA and EGDMA and (b) core diameters calculated from particle diameters (assumption w_{Core} = 0.55 be uniform for all particles). Total count of particles: 434.

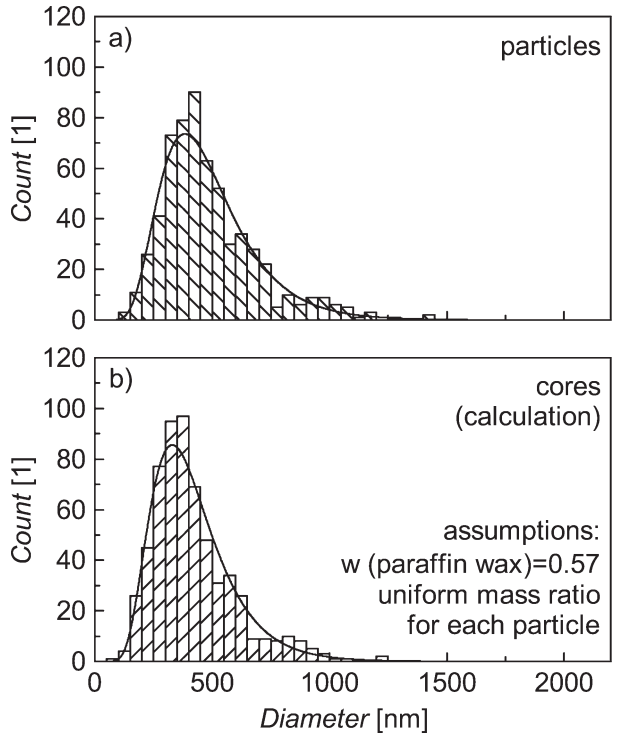

Figure 6. Histograms and overlaid logarithmic normal-distribution of (a) diameters of particles with a wax core and a shell made of MMA, iBoMA, and EGDMA and (b) core diameters calculated from particle diameters (assumption w_{Core} = 0.57 be uniform for all particles). Total count of particles: 609.

Table II. Paraffin Wax Content (w_{Core}) Along with the Mean and Median of the Actually Detected Capsule Diameters ($d_{Capsule}$) and the Calculated Core Diameters (d_{Core}) of Capsules with Polymeric Shell Obtained from Different Monomer Mixtures

		$d_{Capsule}$ (nm)		d_{Core} (nm)	
Monomer mixture	w_{Core} (%)	Mean	Median	Mean	Median
MMA/EGDMA	55	354	280	301	238
MMA/iBoMA/EGDMA	57	487	439	419	377

In TSFD scattering domains with diameters between 200 and 400 nm are most efficient.[14] However, studies showed that domains with diameters up to 1000 nm are highly efficient in terms of backscattering.[14] From this point of view the particles produced within this study are rather promising for application in TSFD. Furthermore, the established encapsulation process is promising for larger-scale applications with regard to its reasonably low time demand.

TSFD FORMULATED WITH ENCAPSULATED PARAFFIN WAX

Experimental

TSFD Formulation. Resin matrix was prepared by mixing 57 wt % oligomer (Ebecryl 800), 40 wt % reactive diluent (OTA-480), and 3 wt % photo-initiator (Lucirin TPO-L). Employed oligomer and reactive diluent were supplied by Allnex Belgium SA/NV (formerly Cytec Surface Specialities; Drobenbos, BE). Photo-initiator was provided by BASF. The amount of capsules ($m_{Capsules}$) required to maintain a thermotropic additive content ($w_{Additive}$) of 5 wt % in a TSFD formulated with a specific amount of resin matrix was calculated according to eq. (3). This amount of capsules was added to the resin matrix and dispersed subsequently. The resulting mixtures were poured in the intervening space between two glass panes, which were sealed around the edge. Subsequently, the layers were cured by UV-radiation (dose: 8.3 mJ cm^{-2}) from 366 nm bulb of Universal-UV-Lamp (Camag, Muttenz, CH). Removal of the glass panes resulted in ~900 μm thick free-standing layers.

$$m_{Capsules} = m_{Matrix} * \left(\frac{w_{Core}}{w_{Additive}} - 1 \right)^{-1} \quad (3)$$

Determination of Light-Shielding Efficiency. Overheating protection performance of TSFD was determined applying UV/Vis/NIR spectrometry. A double beam UV/Vis/NIR spectrophotometer Lambda 950 (Perkin Elmer, Waltham, MA) equipped with an Ulbricht-sphere (diameter 150 mm) was employed. For the given measurement apparatus the radiation passing through (transmittance) the specimen outside a cone of ~5° relative to the incident beam direction was defined as diffuse (scattered) component. Hemispheric and diffuse transmittance was recorded at normal incidence in the spectral region from 250 to 2500 nm. The integral solar transmittance was determined by weighting the recorded spectral data in steps of 5 nm by the AM1.5 global solar irradiance source function. The spectrophotometer was adapted by a heating stage to adjust sample temperature within a range from ambient temperature to maximum 115°C. Measurements were performed in steps of 5°C. Prior to measurement, the samples were allowed to equilibrate for 5 min at the selected temperature. The heating stage was equipped with a control system consisting of a heating stage-internal J-type thermocouple as temperature sensor and the control unit HS-W-35/M (Heinz Stegmeier Heizelemente HS-Heizelemente GmbH, Fridingen, DE). Within the heating stage the sample was positioned in close proximity of the port hole of the Ulbricht-sphere. *In situ* front- and backside sample surface temperatures as a function of set-point value of the control unit were recorded on a prototype sample with a two-channel temperature measurement instrument T900 (Dostmann electronic GmbH, Wertheim-Reicholzheim, DE) equipped with a precision K-type thermocouple. Sample temperature was assumed as the average of both recorded surface temperatures. Required set-point values to maintain average sample temperatures were calculated from a second order polynomial fit of the temperatures recorded in measurements of the prototype sample.

RESULTS AND DISCUSSION

In Figure 7 the solar hemispheric (square symbol) and solar diffuse (triangle symbol) transmittance of TSFD formulated with

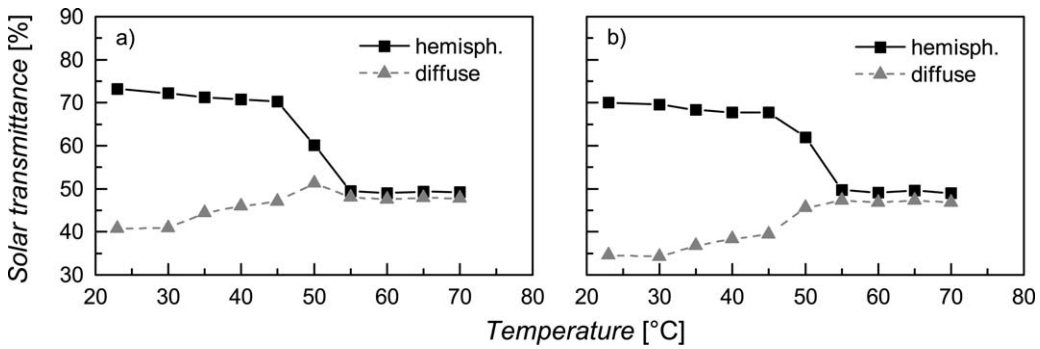

Figure 7. Solar hemispheric (square symbol) and solar diffuse (triangle symbol) transmittance as a function of temperature of TSFD formulated with 5 wt % thermotropic additive content. Thermotropic additive was incorporated in encapsulated form with a polymeric shell obtained from different monomer mixtures, either (a) MMA and EGDMA or (b) MMA, iBoMA, and EGDMA.

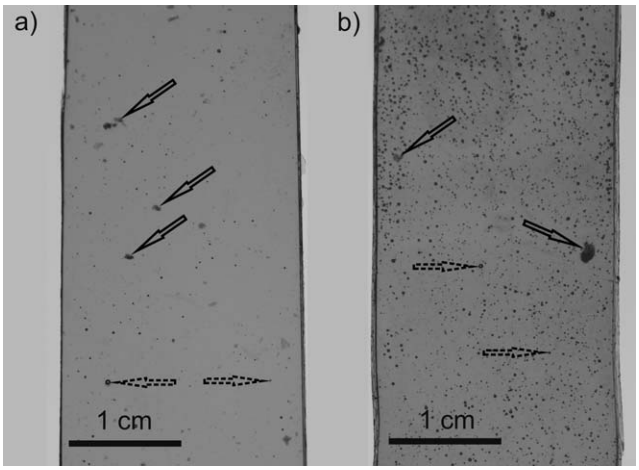

Figure 8. Photographs of TSFD containing capsules with a polymeric shell resulting from either (a) MMA and EGDMA or from (b) MMA, iBoMA, and EGDMA. Visible inhomogeneities in the layers are aggregates (solid arrows are pointing on some of them), and macroscopic voids (broken arrows are pointing on some of them). The latter are resulting from manufacturing. The photographs were taken against a cloudy sky.

encapsulated paraffin wax with a polymeric shell obtained from either MMA and EGDMA [Figure 7(a)] or MMA, iBoMA, and EGDMA [Figure 7(b)] is displayed. Both layers exhibited a distinct reduction in solar hemispheric transmittance upon exceeding the switching threshold (45°C). The layer formulated with encapsulated paraffin wax with a polymeric shell obtained from MMA and EGDMA showed a reduction in solar hemispheric transmittance from 73.1 (room temperature) to 49.2% (70°C). At the same time, the solar diffuse transmittance increased from 40.7 (room temperature) to 47.8% (70°C). The layer formulated with encapsulated paraffin wax with a polymeric shell obtained from MMA, iBoMA, and EGDMA showed a reduction in solar hemispheric transmittance from 70.1 (room temperature) to 49.0% (70°C). At the same time, the solar diffuse transmittance increased from 34.6 (room temperature) to 46.8% (70°C). To validate these results, two additional replicates of each individual TSFD were characterized with regard to their overheating protection performance. The replicate measurements were conducted at room temperature and 70°C only. Mean and standard deviation of solar hemispheric and diffuse transmittance were calculated for room temperature and 70°C. The results are presented in Table III. The TSFD formulated with the additive capsules with a polymeric shell obtained from MMA and EGDMA displayed higher solar hemispheric transmittance at room temperature (72.6%) than the TSFD formulated with the additive capsules with a polymeric shell obtained from MMA, iBoMA, and EGDMA (68.6%). However, the achieved solar hemispheric transmittance at 70°C was rather similar for both layers (48.9 vs. 48.7%). The solar diffuse transmittance of both layers increased slightly upon exceeding the threshold temperature (from 38.8 to 47.4% and from 35.3 to 46.6%, respectively).

Figure 8 displays photographs of two TSFD formulated with encapsulated paraffin wax with a polymeric shell obtained either from MMA and EGDMA [Figure 8(a)] or MMA, iBoMA, and EGDMA [Figure 8(b)]. The photographs were taken against a cloudy sky. Several inhomogeneities were observable. Aggregates of the not entirely dispersible capsule powder were detected (solid arrows are pointing on some of them). Furthermore, macroscopic voids which were resulting from the mixing, casting, and curing procedure were evident (broken arrows are pointing on some of them). Some of them were air bubbles generated during casting, others might be generated because of shrinkage of the matrix during curing.

Consequently, the difference in solar hemispheric transmittance at room temperature detected for these two TSFD may be ascribed to a multitude of factors like slight differences in shell-material content, refractive index differences between matrix/shell/additive, slight differences in size distribution or the higher concentration of voids in the layers formulated with encapsulated paraffin wax with a polymeric shell obtained MMA, iBoMA, and EGDMA.

Anyway, compared to earlier results, a remarkable improvement in overheating protection performance of TSFD was obtained. A TSFD produced from the same matrix and additive type, but additive not being encapsulated (referred to as M7A1-OTA-p3-RT-0.008[22] exhibited a reduction in solar hemispheric transmittance from 81.2 (room temperature) to 78.5% (70°C). That was ascribed to the inappropriate diameters of spherical scattering domains formed by the additive, ranging from 2.76 to 116 μm.

Thus, the better light-shielding efficiency of the TSFD formulated with encapsulated additive was ascribed to the rather optimal diameter of the scattering domains. However, the detected solar hemispheric transmittance at room temperature of around 70% is significantly lower as compared to the result of 81.2% detected for the TSFD formulated with the additive not being encapsulated.[22] This may be ascribed to the differences in scattering domain size: For scattering domains that are too big for optimal back-scattering, a low potential refractive index difference between matrix and additive probably yields no distinct

Table III. Mean and Standard Deviation (the Latter in Brackets) of Solar Hemispheric and Diffuse Transmittance Detected at Room Temperature and 70°C of TSFD Formulated with Encapsulated Paraffin Wax with Polymeric Shell Obtained from Different Monomer Mixtures (Results from Threefold Determination)

	Solar transmittance at room temperature		Solar transmittance at 70°C	
Monomer mixture	Hemisph. (%)	Diffuse (%)	Hemisph. (%)	Diffuse (%)
MMA/EGDMA	72.6 (0.5)	38.8 (1.7)	48.9 (0.2)	47.4 (0.3)
MMA/iBoMA/EGDMA	68.6 (1.3)	35.3 (0.8)	48.7 (0.3)	46.6 (0.2)

effect on solar hemispheric transmittance at room temperature due to low back-scattering efficiency. However, for layers formulated with optimally sized scattering domains, even a small refractive index difference between matrix and additive may yield a significant effect on solar hemispheric transmittance (i.e., a lower transmittance) at room temperature due to high back-scattering efficiency. Thus, future work also has to address the optimization of the matrix/additive combination more in detail.

CONCLUSION AND OUTLOOK

Within this study, a photo-initiated miniemulsion polymerization technique was established in order to encapsulate a thermotropic additive with a polymeric acrylate shell and thereby obtain optimally sized scattering domains for formulation of TSFD. The light-shielding efficiency of the TSFD formulated with these capsules was significantly improved as compared to layers lacking scattering domains with adjusted size. The improvements in light-shielding efficiency of TSFD were rather remarkable. The obtained solar hemispheric transmittances were around 73 and 49% at temperatures below and above the switching threshold, respectively. However, efficient overheating protection of an all polymeric flat plate collector requires solar hemispheric transmittances of >85 and $<60\%$ at temperatures below and above the switching threshold, respectively.[9] An improvement in light-shielding efficiency of the layers is probably achievable upon optimization of matrix/additive combination. The lower the refractive index difference at room temperature is, the higher the corresponding solar hemispheric transmittance will be. Thus, future work has to focus on an optimization of material composition of matrix and polymeric shell in order to match the refractive index of thermotropic additive at room temperature as good as possible.

Anyway, the established miniemulsion polymerization routine would also allow for encapsulation of thermotropic additives with different melting points rather easily and thus easy adjustment of switching threshold of TSFD formulated with these capsules (e.g., by utilization of a spinning disk reactor[85]). With regard to encapsulation of thermotropic additives with higher melting temperature, monomer evaporation is an issue, thus carrying out the reaction in pressurized atmosphere (oxygen-free) would be beneficial in order to mitigate monomer losses. Anyway, a major advantage of the photo-initiated process is the process acceleration. The duration of the established photo-initiated polymerization was 15 min.

ACKNOWLEDGMENTS

The research work of this paper was performed at the Polymer Competence Center Leoben GmbH (PCCL, Austria) within the framework of the COMET-program of the Federal Ministry for Transport, Innovation and Technology, and Federal Ministry for Econoomy, Family and Youth with contributions by University of Leoben (Department Polymer Engineering and Science, Leoben AT). The PCCL is funded by the Austrian Government and the State Governments of Styria and Upper Austria. Parts of this research project are funded by the State Government of Styria, Department Zukunftsfonds (Project number 5019).

The authors want to express their gratitude to Sandra Schlögel and Jakob Manhart (PCCL) for their help upon setting up laboratory equipment, to Thomas Grießer and Mathias Edler (Christian Doppler Laboratory for Functional and Polymer Based Inkjet Inks at University of Leoben, Department Polymer Engineering and Science, Chemistry of Polymeric Materials, Leoben, AT) for providing the ultrasound device and to Carina Tauterer (University of Leoben, Department of Environmental and Energy Process Engineering, Institute of Waste Treatment Technologies and Landfilling) for providing the freeze drying apparatus.

Furthermore, the contribution of materials by Allnex Belgium SA/NV (formerly Cytec Surface Specialities; Drogenbos, BE), BASF SE (Ludwigshafen, DE), and Sasol Wax GmbH (Hamburg, DE) are gratefully acknowledged.

REFERENCES

1. Nitz, P.; Hartwig, H. *Sol. Energy* **2005**, *79*, 573–582.
2. Seeboth, A.; Schneider, J.; Patzak, A. *Sol. Energy Mater. Sol. Cells* **2000**, *60*, 263.
3. Yao, J.; Zhu, N. *Build. Environ.* **2012**, *49*, 283.
4. Inoue, T. *Energy Build.* **2003**, *35*, 463.
5. Hartwig, H. Konzepte für die Integration selbstregelnder, thermotroper Schichten in moderne Gebäudehüllen zur passiven Nutzung der Sonnenenergie. Dissertation, Technische Universität München, München, July **2003**.
6. Nitz, P.; Wagner, A. *BINE Themeninfo.* **2002**, I/02, 1.
7. Resch, K.; Hausner, R.; Wallner, G. M. In Proceedings of ISES Solar World Congress 2007, Solar Energy and Human Settlement; Goswami, D. Y., Zhao, Y., Eds.; Springer: Berlin; **2007**, pp 561–565.
8. Resch, K.; Wallner, G. M. *Sol. Energy Mater. Sol. Cells* **2009**, *93*, 119.
9. Wallner, G. M.; Resch, K.; Hausner, R. *Sol. Energy Mater. Sol. Cells* **2008**, *92*, 614.
10. Harrison, S.; Cruickshank, C. A. *Energy Proc.* **2012**, *30*, 793.
11. Kalogirou, S. A. *Prog. Energy Combust. Sci.* **2004**, *30*, 231.
12. Resch, K.; Hausner, R.; Wallner, G. M.; Lang, R. W. In Polymeric Materials for Solar Thermal Applications; Köhl, M.; Meir, M. G.; Papillon, P.; Wallner, G. M.; Saile, S., Eds.; Wiley-VCH: Weinheim, **2012**; pp 255–266.
13. Resch, K.; Weber, A. *Berg- Huettenmaenn. Monatsh.* **2011**, *156*, 429.
14. Nitz, P. Optical modelling and characterisation of thermotropic systems. Dissertation, Albert Ludwigs Universität, Freiburg i.B., August **1999**.
15. Gruber, D. P.; Resch, K. Thermotropic overheating protection glazings: Scattering simulation and theoretical optimization of performance characteristic, in preparation.
16. Resch, K.; Wallner, G. M.; Hausner, R. *Sol. Energy* **2009**, *83*, 1689.
17. Resch, K.; Wallner, G. M.; Lang, R. W. *Macromol. Symp.* **2008**, *265*, 49.
18. Ruhmann, R.; Seeboth, A.; Muehling, O.; Loetzsch, D. *AST* **2012**, *77*, 124.

19. Weber, A.; Resch, K. *Energy Proc.* **2012**, *30*, 471.
20. Weber, A.; Resch, K. *J. Appl. Polym. Sci.* **2014**, *131*, 39950.
21. Weber, A.; Schmid, A.; Resch, K. *J. Appl. Polym. Sci.* **2014**, *131*, 39910.
22. Weber, A.; Schlögl, S.; Resch, K. *J. Appl. Polym. Sci.* **2013**, *130*, 3299.
23. Weber, A.; Resch, K. *J. Polym. Eng.*, accepted.
24. Muehling, O.; Seeboth, A.; Haeusler, T.; Ruhmann, R.; Potechius, E.; Vetter, R. *Sol. Energy Mater. Sol. Cells* **2009**, *93*, 1510.
25. Resch, K.; Wallner, G. M. *Polym. Adv. Technol.* **2009**, *20*, 1163.
26. Weber, A.; Resch, K. *J. Polym. Res.* **2012**, *19*, 1.
27. Resch, K. Polymeric Thermotropic Materials for Overheating Protection of Solar Collectors. Dissertation, University of Leoben, Leoben, October **2008**.
28. Alay, S.; Alkan, C.; Göde, F. *Thermochim. Acta* **2011**, *518*, 1.
29. Alkan, C.; Sarı, A.; Karaipekli, A. *Energy Convers. Manage.* **2011**, *52*, 687.
30. Alkan, C.; Sarı, A.; Karaipekli, A.; Uzun, O. *Sol. Energy Mater. Sol. Cells* **2009**, *93*, 143.
31. Chen, C.; Chen, Z.; Zeng, X.; Fang, X.; Zhang, Z. *Colloid Polym. Sci.* **2012**, *290*, 307.
32. Chen, Z.-H.; Yu, F.; Zeng, X.-R.; Zhang, Z.-G. *Appl. Energy* **2012**, *91*, 7.
33. Cortazar, M. G. de; Rodríguez, R. *J. Appl. Polym. Sci.* **2013**, *127*, 5059.
34. Delgado, M.; Lázaro, A.; Mazo, J.; Zalba, B. *Renew. Sust. Energy Rev.* **2012**, *16*, 253.
35. Fang, Y.; Kuang, S.; Gao, X.; Zhang, Z. *Energy Convers. Manage.* **2008**, *49*, 3704.
36. Luo, Y.; Zhou, X. *J. Polym. Sci. Part A: Polym. Chem.* **2004**, *42*, 2145.
37. Ma, S.; Song, G.; Li, W.; Fan, P.; Tang, G. *Sol. Energy Mater. Sol. Cells* **2010**, *94*, 1643.
38. Ma, Y.; Chu, X.; Li, W.; Tang, G. *Sol. Energy* **2012**, *86*, 2056.
39. Qiu, X.; Li, W.; Song, G.; Chu, X.; Tang, G. *Sol. Energy Mater. Sol. Cells* **2012**, *98*, 283.
40. Qiu, X.; Li, W.; Song, G.; Chu, X.; Tang, G. *Energy* **2012**, *46*, 188.
41. Qiu, X.; Song, G.; Chu, X.; Li, X.; Tang, G. *Sol. Energy* **2013**, *91*, 212.
42. Qiu, X.; Song, G.; Chu, X.; Li, X.; Tang, G. *Thermochim. Acta* **2013**, *551*, 136.
43. Sarı, A.; Alkan, C.; Karaipekli, A. *Appl. Energy* **2010**, *87*, 1529.
44. Sarier, N.; Onder, E. *Thermochim. Acta* **2012**, *540*, 7.
45. Shirin-Abadi, A. R.; Mahdavian, A. R.; Khoee, S. *Macromolecules* **2011**, *44*, 7405.
46. Wang, Y.; Shi, H.; Xia, T. D.; Zhang, T.; Feng, H. X. *Mater. Chem. Phys.* **2012**, *135*, 181.
47. Zhao, C.; Zhang, G. *Renew. Sust. Energy Rev.* **2011**, *15*, 3813.
48. Amrhein, P.; Spannagel, A.; Ascherl, H.; Lang-Wittkowski, G. (BASF AG). Patent WO 2006092439A1, March 3 **2006**.
49. Rodriguez Romero, J. F.; Sanchez Silva, M. L.; Sanchez Parades, P.; De Lucas Martinez, A.; Torres Barreto, M. L. Universidad de Castilla-La Mancha; Asintec, Asociacion para la Incorporation de nuevas Tecnologias a la Empresa, Patent WO 2007107171A1, March 23 **2006**.
50. Schröder-Grimonpont, T.; Willax, H.; Katz, B.; Brust, J.; Altmann, S.; Schmidt, M. (BASF SE). Patent WO 2012110443A1, February 13 **2012**.
51. Cao, Z.; Ziener, U. *Curr. Org. Chem.* **2013**, *17*, 30.
52. Hecht, L. L.; Wagner, C.; Landfester, K.; Schuchmann, H. P. *Langmuir* **2011**, *27*, 2279.
53. Hecht, L. L.; Wagner, C.; Özcan, Ö.; Eisenbart, F.; Köhler, K.; Landfester, K.; Schuchmann, H. P. *Macromol. Chem. Phys.* **2012**, *213*, 2165.
54. Koroleva, M. Y.; Yurtov, E. V. *Russ. Chem. Rev.* **2012**, *81*, 21.
55. Landfester, K. *Macromol. Rapid Commun.* **2001**, *22*, 896.
56. Landfester, K.; Schork, F.; Kusuma, V. A. *C. R. Chim.* **2003**, *6*, 1337.
57. Landfester, K. *Angew. Chem.* **2009**, *121*, 4556.
58. Landfester, K.; Weiss, C. K. In Advances in Polymer Science: Modern Techniques for Nano- and Microreactors/-reactions; Caruso, F., Ed.; Springer: Berlin, **2010**, pp 1–49.
59. Rao, J. P.; Geckeler, K. E. *Prog. Polym. Sci.* **2011**, *36*, 887.
60. van Zyl, A. J.; Wet-Roos, D. d.; Sanderson, R. D.; Klumperman, B. *Eur. Polym. J.* **2004**, *40*, 2717.
61. Schork, F. J.; Luo, Y.; Smulders, W.; Russum, J. P.; Butté, A.; Fontenot, K. In Advances in Polymer Science: Polymer Particles; Okubo, M., Ed.; Springer: Berlin, **2005**; Vol. *175*, pp 129–255.
62. Seok Kwon, O.; Jang, J.; Bae, J. *Curr. Org. Chem.* **2013**, *17*, 3.
63. Tiarks, F.; Landfester, K.; Antonietti, M. *Langmuir* **2001**, *17*, 908.
64. Landfester, K.; Bechthold, N.; Förster, S.; Antonietti, M. *Macromol. Rapid Commun.* **1999**, *20*, 81.
65. Antonietti, M.; Landfester, K. *Prog. Polym. Sci.* **2002**, *27*, 689.
66. Asua, J. M. *Prog. Polym. Sci.* **2002**, *27*, 1283.
67. Abismaïl, B.; Canselier, J.; Wilhelm, A.; Delmas, H.; Gourdon, C. *Ultrason. Sonochem.* **1999**, *6*, 75.
68. Canselier, J. P.; Delmas, H.; Wilhelm, A. M.; Abismaïl, B. *J. Dispersion Sci. Technol.* **2002**, *23*, 333.
69. Walstra, P. *Chem. Eng. Sci.* **1993**, *48*, 333.
70. Chemtob, A.; Kunstler, B.; Croutxé-Barghorn, C.; Fouchard, S. *Colloid Polym. Sci.* **2010**, *288*, 579.
71. Seferis, J. C. In Polymer Handbook; Brandrup, J., Immergut, E. H., Grulke, E. A., Eds.; Wiley: New York, **1999**; pp VI/571–VI/582.
72. Chen, W.; Chang, C. *J. Mater. Chem.* **1999**, *9*, 2307.
73. Slone, R. V. *Encyclopedia of Polymer Science and Technology.* Wiley: Hoboken, **2010**, DOI: 10.1002/0471440264.pst196.pub2.

74. Ehrenstein, G. W.; Pongratz, S. Beständigkeit von Kunststoffen; Hanser: München, **2007**.
75. Landfester, K.; Bechthold, N.; Tiarks, F.; Antonietti, M. *Macromolecules* **1999**, *32*, 5222.
76. Landfester, K.; Bechthold, N.; Tiarks, F.; Antonietti, M. *Macromolecules* **1999**, *32*, 2679.
77. Freund, M.; Csikós, R.; Keszthelyi, S.; Mózes, G. In Developments in Petroleum Science; Mózes, G., Ed.; Akadémiai Kiadó: Budapest, **1982**; Vol. *14*, pp 1–336.
78. Ehrenstein, G. W. Polymer-Werkstoffe: Struktur – Eigenschaften – Anwendung; Hanser: München, **2011**.
79. Baur, E.; Brinkmann, S.; Osswald, T. A.; Schmachtenberg, E. Saechtling-Kunststoff-Taschenbuch; Hanser: München, **2007**.
80. Hellerich, W.; Harsch, G.; Haenle, S. Werkstoff-Führer Kunststoffe: Eigenschaften, Prüfungen, Kennwerte; Hanser: München, **2010**.
81. Hummel, D. O. Atlas of plastics additives: Analysis by spectrometric methods; with 62 tables; Springer: Berlin, **2002**.
82. Günzler, H.; Heise, H. M. IR-Spektroskopie: Eine Einführung; VCH: Weinheim, **1996**.
83. Verleye, G. A. L.; Roeges, N. P. G.; Moor, M. O. de. Easy identification of plastics and rubbers; Rapra Technology: Shrewsbury, UK, **2001**.
84. Socrates, G. Infrared and Raman Characteristic Group Frequencies; Wiley: Chichester, **2001**.
85. Pask, S. D.; Nuyken, O.; Cai, Z. *Polym. Chem.* **2012**, *3*, 2698.